JACS
JOURNAL OF THE AMERICAN CHEMICAL SOCIETY
pubs.acs.org/JACS
Article

Electrosynthesis of Unusual Nonfcc Palladium Hydride Nanoparticles

Jaeyoung Hong and Xiao Su*

Cite This: J. Am. Chem. Soc. 2024, 146, 18586−18591
Read Online
ACCESS | Metrics & More | Article Recommendations | Supporting Information

ABSTRACT: Intercalation of hydrogen into the palladium atomic layers during the growth of Pd nanoparticles can lead to the synthesis of unique palladium hydride phases. Here, we discover an unusual nonfcc palladium hydride nanoparticle, a structure that is not face-centered cubic (fcc), formed through coreduction of water molecules and Pd ions in solution. Crystal structure determination based on atomic electron tomography points to potential triclinic unit cells, indicating the presence of more than one nonfcc phase, with some of those being a stack of loosened and distorted close-packed layer of atoms. The probability of finding the nonfcc phase in single-crystalline particles varies depending on the number and distribution of contact area with other particles. Roughly half of the isolated and one side-coalesced single-crystal particles exhibit a nonfcc structure, while fcc dominates multiple side-coalesced single crystals as well as polycrystal particles. These observations suggest a coalescence-induced phase transition from a nonfcc to a stable fcc structure, due to the metastable nature of the nonfcc phases. While hydrogen is proven to be a key component for the synthesis of the nonfcc structure, there was limited formation of the unusual phase in a H_2 gas bubbling system. Thus, electrochemical pathways can be promising for the in situ creation and study of unique metastable nanomaterials.

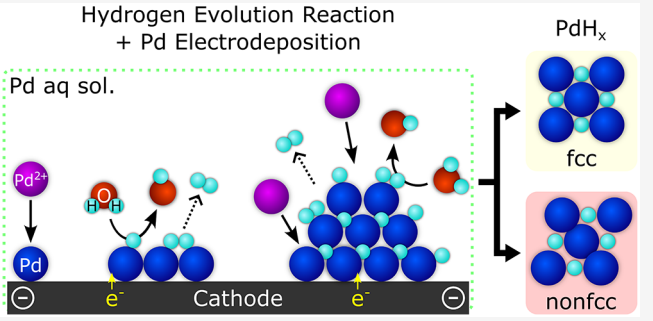

1. INTRODUCTION

The recent discovery of metastable hexagonal close-packed (hcp) palladium hydride (PdH_x) nanoparticles synthesized in the liquid transmission electron microscopy (TEM) cell has proved that reduction of Pd ions in a hydrogen-rich environment can result in the evolution of previously unreported metastable phases.[1] Electron beam irradiation in a liquid cell dissociates water molecules to make several chemical products including hydrated electrons and hydrogen species, which serve as reducing agents and hydrogen sources, respectively. However, the hcp PdH_x phase is not easily reproducible outside a TEM, with the reported synthesis limited to a liquid cell under special conditions that enable the vigorous radiolysis of water. Thus, synthetic approaches of Pd that can generate these unusual phases, without the need for electron beam-induced radiolysis, are highly desirable for the fundamental study and eventual modular production of these metastable particles. In the pursuit of a modular hydrogen-rich synthesis approach that is nonreliant on these constraining radiolysis conditions, we discovered a distinct and unique nonfcc PdH_x through the electrochemical coreduction of water and Pd ions.

The concept relies on an electrochemical system to provide in situ a reducing agent and hydrogen through charge transfer from an electrode to the aqueous solution containing Pd (Figure 1). An applied negative potential induces both hydrogen evolution reaction (HER) ($2H^+(aq) + 2e^- \rightarrow H_2(g)$, −0.23 V vs Ag/AgCl at pH 0, and $2H_2O(l) + 2e^- \rightarrow H_2(g) + 2OH^-(aq)$, −1.06 V vs Ag/AgCl at pH 14) and reduction of Pd precursor tetrachloropalladate ($PdCl_4^{2-}(aq)$ +

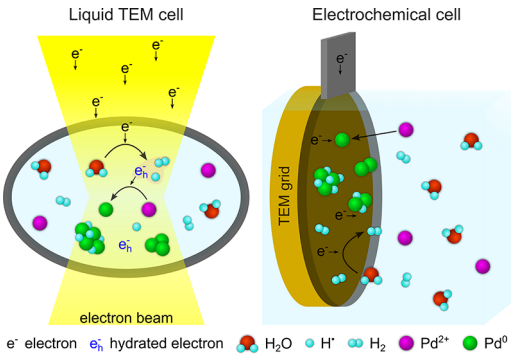

Figure 1. Graphical representation of the liquid TEM cell used for hcp PdH_x nanoparticle synthesis and the electrochemical system used in this study.

Received: April 8, 2024
Revised: June 6, 2024
Accepted: June 7, 2024
Published: July 1, 2024

https://doi.org/10.1021/jacs.4c04826
J. Am. Chem. Soc. 2024, 146, 18586−18591

$2e^- \rightarrow Pd(s) + 4Cl^-(aq)$, 0.361 V vs Ag/AgCl).[2] Considering the evolution of hcp PdH_x in a high H-to-Pd ratio environment,[1] the presence of a large amount of hydrogen during the electrodeposition of Pd ions is required for the investigation of the emergence of an unconventional hydride phase. In this context, constant current was forced to flow through a working electrode to secure a certain degree of H_2 production along with Pd reduction, especially since the Pd reduction current is limited by the diffusion of Pd ions at high overpotentials.[3] Constant current density from −1.5 to −30 mA/cm^2 was applied to the system, resulting in potentials ranging from −1.2 to −1.8 V vs Ag/AgCl (Figure S1). An acidic electrolyte with pH 3.3 was used to prevent aggregation of the deposited particles.

2. RESULTS AND DISCUSSION

2.1. Structural and Chemical Characterization of Electrodeposited Nonfcc PdH_x Nanoparticles. High-resolution TEM (HRTEM) images of the nanoparticles formed on electrodes exhibited zone axis diffraction patterns that do not belong to conventional fcc Pd and PdH_x. These patterns were categorized into 12 cases plus a distorted fcc-like case, a fcc with forbidden reflection-like case,[4] and a rarely observed case (Figures 2 and S2) with variance in *d*-spacings suspected to be originated from different amounts of hydrogen in the particles. While diffraction pattern cases 4, 5, and 12 resembled $[1\bar{2}1\bar{3}]$, [0001], and $[01\bar{1}1]$ zone axis diffraction patterns of hcp PdH_x, respectively,[1] the characteristic $[\bar{2}110]$ zone axis diffraction pattern of the hcp structure was not observed (Figure S3). Considering that characteristic ABAB stacking of atomic layers in the hcp structure can be validated in a hcp crystal aligned at the $[\bar{2}110]$ zone axis, the hcp phase was presumed to be not present on the electrodes. Besides, distorted fcc-like case resembled the [110] zone axis diffraction pattern of fcc with a *d*-spacing of one (111) spot larger than that of the other or with *d*-spacings of both (111) spots larger than those in typical *β*-PdH_x. Fcc with a forbidden reflection-like case was not very distinguishable from the fcc [112] zone axis diffraction pattern with forbidden reflections $1/2(1\bar{3}1)$,[4] which also resembled the pattern of case 5 with two sets of dim spots. While these features made structure determination challenging, the electrochemical route to synthesis provided a platform for the creation of unique, unusual crystal structures.

Energy-dispersive X-ray spectroscopy (EDS) spectra confirmed that the nonfcc particle is made of Pd with a small amount of oxygen presumably on the particle surface, which might have come from hydroxyl ions formed during HER, oxygen dissolved in the solution, or oxygen in the air (Figure 3a,b). Moreover, a peak appeared at ∼4.5 eV in electron energy loss spectroscopy (EELS) spectra of the nonfcc particles demonstrated that the nonfcc phase is PdH_x as the peak resembles the characteristic plasmon peak of fcc *β*-PdH_x[5,6] (Figures 3c,d and S4).

2.2. Crystal Structure Determination of Nonfcc Particles Based on Atom Electron Tomography (AET). To elucidate the crystal structure of the nonfcc particles, atom electron tomography (AET) with the real-space iterative reconstruction (RESIRE) reconstruction algorithm was applied to the data.[7,8] The application of AET was necessary as selected area electron diffraction (SAED) analysis was inapplicable due to the overlap of *d*-spacings of nonfcc and fcc phases as well as the low intensity of nonfcc diffraction spots owing to the low portion of the nonfcc phase, which will

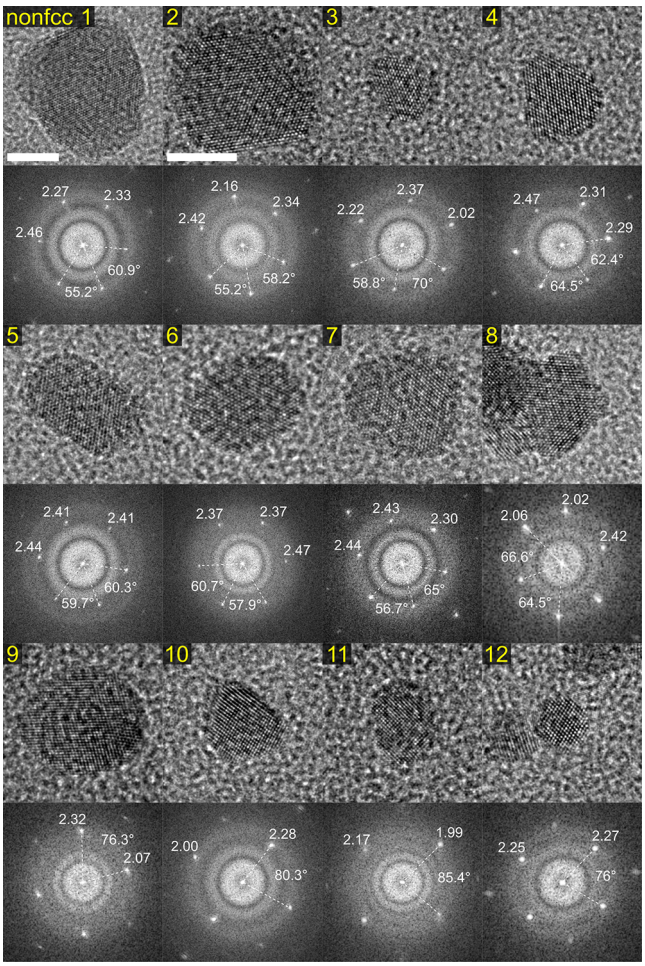

Figure 2. Structural analysis of nonfcc particles electrochemically deposited on TEM grids via HRTEM images and their diffraction patterns obtained by fast Fourier transform (fft). Interplanar distances (Å units) and angles between neighboring diffraction spots are represented in diffraction patterns. Diffraction pattern case number is denoted on the top left corner of HRTEM images. Magnification of images without a scale bar is equal to that of the case 2 image. Scale bars, 5 nm.

be discussed in detail in Sections 2.3 and 2.5 (Figure S5). It was noted that the particles with a nonfcc structure were deformed over the tilt series acquisition due to the electron irradiation needed for AET (Figures S6−S10), which led to incoherent atom arrangement in reconstructured particles as represented in Figure S11a. However, reconstruction based on periodicity-amplified tilt series led to a more orderly atom arrangement in reconstructed data, though there was still notable irregular stacking of atomic layers (Figures S11−S16), and local periodic regions present in two reconstructed particles were used as a basis for approximation of a unit cell of the nonfcc phase (Particles 1 and 2 in Figures 4, S11b, and S13b).

Determination of the unit cell was not straightforward owing to the lack of long-range order in the reconstructed data, necessitating the identification of the crystal system of the nonfcc phase in advance. Based on the absence of a diffraction pattern with two different spots with *d*-spacings larger than 1.5 Å in orthogonal relationship and the presence of rhomboid atomic arrangement in the local periodic region of the reconstruction data, the nonfcc phase is proposed to belong

https://doi.org/10.1021/jacs.4c04826
J. Am. Chem. Soc. 2024, 146, 18586−18591

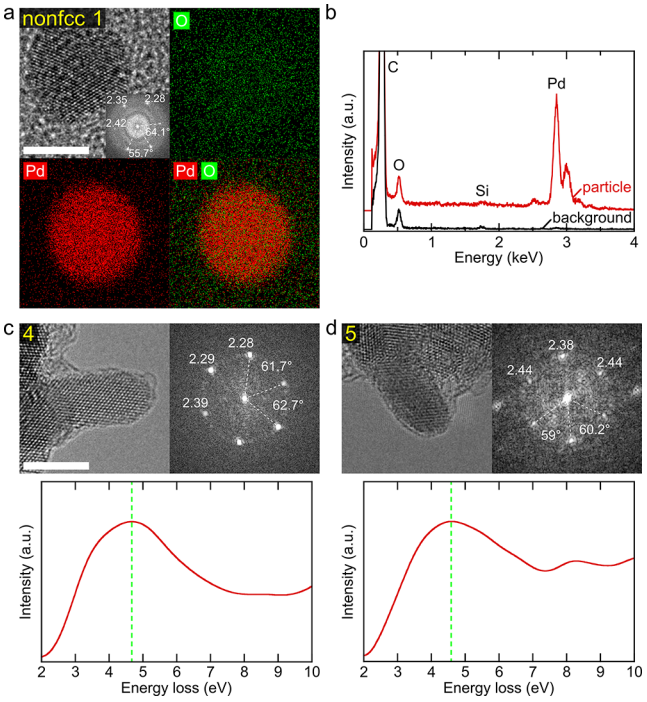

Figure 3. Elemental analysis of nonfcc particles. (a) HRTEM images, diffraction patterns, and EDS maps and (b) EDS spectra of a case 1 nonfcc particle and background carbon film. (c,d) HRTEM images, diffraction patterns, and EELS spectra at the low loss region of case 4 and 5 nonfcc particles, respectively. Interplanar distances are represented in the figures (Å units). a.u., arbitrary units. Scale bars, 5 nm.

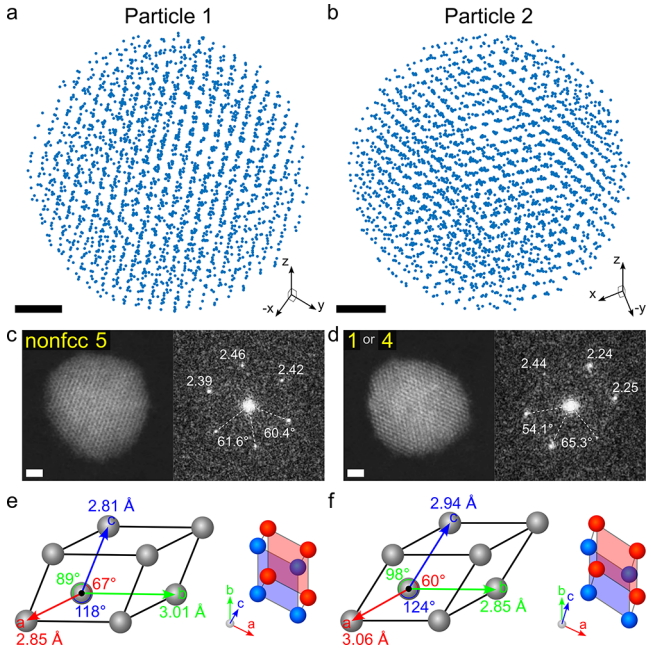

Figure 4. 3D atomic structure of reconstructed nonfcc (a) Particle 1 and (b) Particle 2 with blue dots representing atom positions inside the nanoparticles. The particles viewed from another direction where discontinuous atomic layers were more conspicuous can be found in Figures S11b and S13b. (c,d) High-resolution scanning transmission electron microscopy images and diffraction patterns of Particles 1 and 2. Interplanar distances are represented in the figures (Å units). (e,f) Approximated possible unit cells of Particles 1 and 2 and their projected image onto the basal plane. Red and blue spheres are Pd atoms in the top and bottom layer, respectively. Scale bars, 1 nm.

to the triclinic system. Since every reflection is allowed in the triclinic crystal system, unit cell length parameters cannot be excessively larger than the Pd−Pd bond length in bulk fcc Pd, 2.751 Å,[9] as it would result in a *d*-spacing of crystallographic planes larger than the value observed in HRTEM analysis. In this regard, eight neighboring atoms were selected in a local periodic region of the reconstruction data in a manner in which they compose each corner of a unit cell. Due to the irregularity in the atomic array which was present even in the local periodic region, a range of unit cell parameters were extracted from several sets of eight atoms (Figures S11c and S13c). Based on the lattice parameter range, numerous combinations of the lattice constants were examined to find unit cell candidates of a tilt series using MATLAB. Two zone axis diffraction patterns of each combination were compared with a pattern obtained in the tilt series and an arbitrarily selected pattern in Figure 2, one by one, to find the best match.

As a result, two unit cells were deduced from each reconstructed particle, and one of each is shown in Figure 4. For Particle 1, the lattice parameters were a = 2.85 Å, b = 3.01 Å, c = 2.81 Å, α = 67°, β = 89°, and γ = 118° (Figure 4e), and for Particle 2, the parameters found were a = 3.06 Å, b = 2.85 Å, c = 2.94 Å, α = 60°, β = 98°, and γ = 124° (Figure 4f). The other unit cell candidate of each particle can be found in Figures S17 and S18. Unfortunately, not all unusual diffraction patterns obtained in the HRTEM analysis were resolved by the unit cell candidates even when minor deviation was allowed (Figures 2, S2, S17c,h, and S18c,h), which implied that there could be more than one nonfcc phase on electrodes. Nevertheless, the unit cell structure of the candidates inferred that at least some nonfcc phases are a stack of loosened and distorted close-packed layers (Figures 4e,f, S17a,b,f,g, and S18a,b,f,g). While the deviation from the close-packed structure was suspected to be caused by the impregnation of hydrogen in the Pd matrix, the H fraction x in the nonfcc PdH_x particles could not be estimated owing to the lack of information regarding a unit cell volume of pure Pd with the nonfcc structure, let alone the position of the H atoms in the Pd matrix.

2.3. Coalescence-Induced Transition of the Nonfcc Phase. It was noted that the observance probability of this nonfcc phase was dependent on the morphology of the particles. Electrodeposited nanoparticles were categorized into four groups depending on their conformation: (1) single isolated single-crystalline particle, (2) single-crystalline particle coalesced with other particle(s) only on one side, (3) single-crystalline particle coalesced with other particles on multiple sides, and (4) polycrystalline particle. Probabilities of finding nonfcc phase in single isolated single-crystalline nanoparticles and single-crystalline particles coalesced on one side were similar, being roughly half (Figures 5a,b and 6a,b); ∼65 and ∼56% of analyzed particles in each category exhibited nonfcc phase, for example, when −15 mA/cm^2 of current density flowed to the electrode in a 0.1 mM Pd solution. Meanwhile, nearly all single-crystalline particles coalesced on multiple sides, such as particles located in the inner part of an assemblage of nanoparticles, exhibited an fcc structure (Figure 5c). Likewise, nonfcc structured grain was rarely observed in polycrystal particles, irrespective of whether the particle was in contact with others or not (Figure 5d).

https://doi.org/10.1021/jacs.4c04826
J. Am. Chem. Soc. 2024, 146, 18586−18591

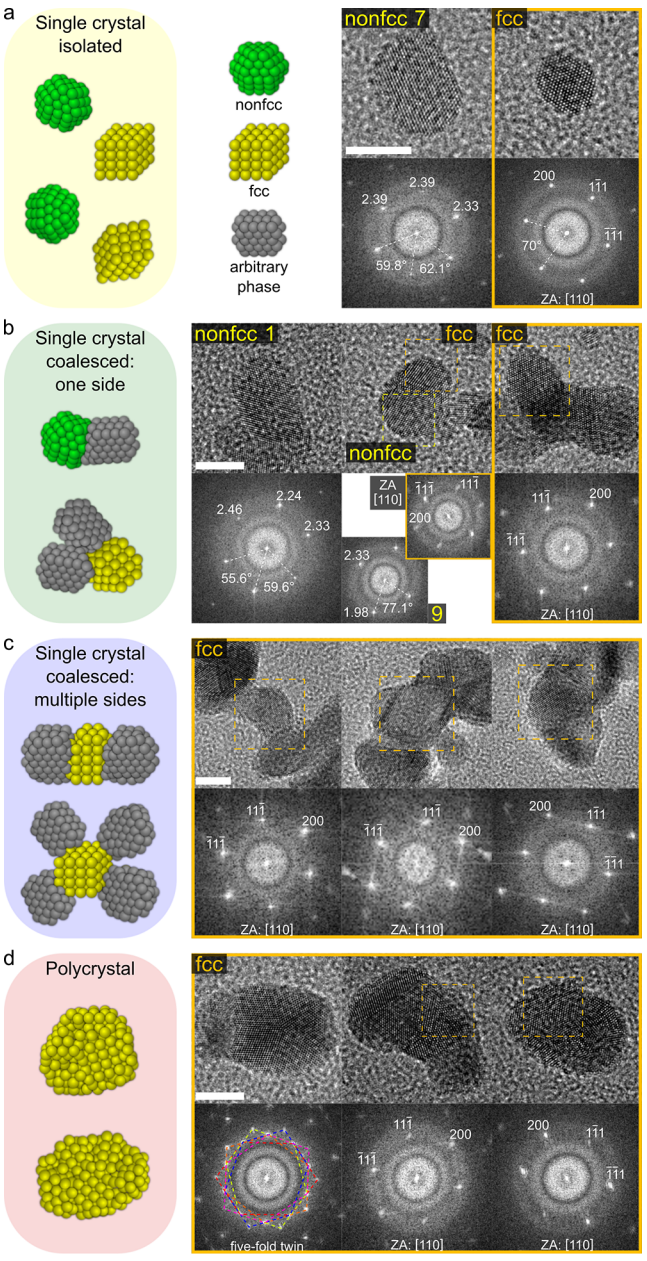

Figure 5. Graphical representation, HRTEM images, and their diffraction patterns of (a) isolated single-crystal particles, (b) coalesced single-crystalline particles coalesced on one side like particles positioned at the surface of agglomerates, (c) single-crystalline particles coalesced on multiple sides like particles positioned inside agglomerates, and (d) polycrystal particles. Interplanar distances are represented in the figures for nonfcc particles (Å units). ZA, zone axis. Scale bars, 5 nm.

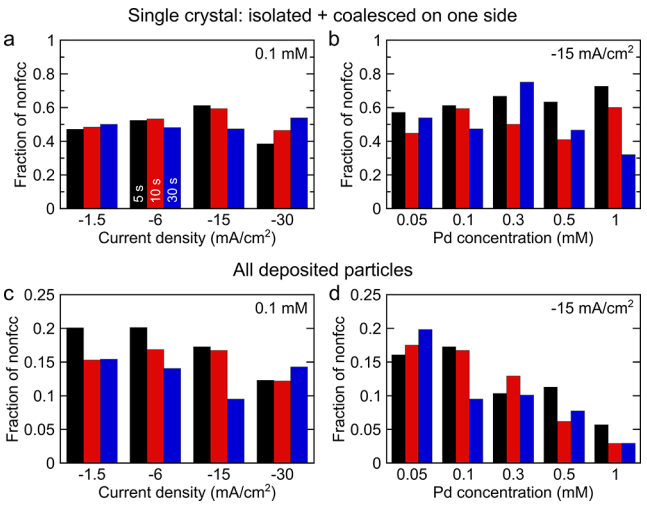

Figure 6. (a,b) Estimated volume fraction of the nonfcc phase for single isolated and one side-coalesced single-crystalline particles as a function of (a) current density in a 0.1 mM Pd solution and (b) Pd concentration with a current density of −15 mA/cm^2. (c,d) Estimated total volume fraction of the nonfcc phase on electrodes as a function of (c) current density in a 0.1 mM solution of Pd and (d) Pd concentration at a current density of −15 mA/cm^2.

Based on this trend, we conjectured that atom rearrangement involved in the coalescence process induces phase transition from nonfcc to fcc due to the metastable nature of the nonfcc phase. Coalescence of two particles can be accompanied by mass redistribution throughout the internal lattice.[10,11] The rearrangement of atoms triggered by the coalescence could assist the metastable atom array relax into a more stable array. When coalescence occurs only on one side of a particle, the driving force for mass redistribution may not be always high enough to induce bulk diffusion. While heat treatment up to 300 °C exposed a certain degree of atomic rearrangement as noted by the slightly changed shapes of the particles, single isolated single-crystalline nonfcc particles did not undergo phase transition to fcc, thus corroborating their structural stability (Figure S19). In contrast, multiple coalescence events happening at two or more sides of a particle may exert a stronger driving force to trigger lattice diffusion that leads to a phase transition toward a more stable phase. This proposed coalescence-assisted phase transition is in line with molecular dynamics simulations that showed the crystallization of two amorphous Pd nanoparticles during coalescence, which was triggered by stress accumulated at the interface.[12]

2.4. Role of Hydrogen in the Formation of Nonfcc Particles. For determination of the dominant factors that enable the evolution of the nonfcc phase, several different synthetic approaches were taken to verify the effects of hydrogen, electrochemical reduction, substrate, and the Pt counter electrode. First of all, an electrochemical potential more positive than the water reduction potential was applied to reduce Pd ions in a relatively hydrogen-poor environment. Nonfcc phase particles were not observed when 0 V vs Ag/AgCl was applied, and about 10% of single isolated and one side-merged single-crystalline particles exhibited nonfcc structure when −0.55 and −0.8 V vs Ag/AgCl were applied (Figure S20). Although protons could be reduced to form H_2 at −0.55 and −0.8 V vs Ag/AgCl given the HER potential in pH 3.3 being −0.43 V vs Ag/AgCl, the amount of hydrogen species that participated in electrochemical reactions under these potentials would be considerably smaller than the amount in the chronopotentiometry experiments (Figures S1 and S20a). Suppressed evolution of the nonfcc phase under these conditions corroborated the significance of the role of hydrogen in the synthesis of this metastable phase. In addition, bubbling pure H_2 gas into Pd solution led to the formation of nanoparticles with a small fraction, assumably less than ∼10%, of single isolated and one side-coalesced single-crystalline particles exhibiting the nonfcc structure (Figure S21). This result indicated that H_2 gas has limited capability in making the

https://doi.org/10.1021/jacs.4c04826
J. Am. Chem. Soc. 2024, 146, 18586−18591

nonfcc phase, which is far less effective than the proposed electrochemical reduction approach. Furthermore, electrochemical deposition of nonfcc particles on a CNT electrode in place of a TEM grid electrode proved that synthesis of the nonfcc phase is not limited to a specific substrate (Figure S22). Likewise, formation of nonfcc particles in experiments with a graphite counter electrode in lieu of Pt wire demonstrated that the Pt counter electrode is not the cause of the metastable phase evolution (Figure S23).

Given all the above, we hypothesize that the metastable phase evolves through the codeposition of H and Pd atoms, and the synthesis of the nonfcc phase is subject to a relative amount of H to Pd, similar to the proposed formation mechanism of hcp PdH_x in a liquid TEM cell.[1] Surface hydrides, $Pd-H_{ads}$, produced during HER[13−16] could experience deposition of H and Pd atoms on it either alternatively or concurrently instead of participating in H_2 production, resulting in H-impregnated Pd nanoparticles with unique structures. Meanwhile, interplay of the reduction of palladium ions by H_2 generated in HER and the formation of $Pd-H_{ads}$ through dissociative adsorption of H_2 on Pd could also lead to the formation of nonfcc PdH_x, as shown in the H_2 gas bubbling experiment.[17,18] It must be noted that whether unique nonfcc seeds were formed or not was unclear due to the challenges in the structural analysis of particles smaller than few nanometers, which could be partially attributed to the weak (or lack of) crystallinity of the particles in the early stages of nucleation and growth.[19,20] Still, the presence of crystallographic planes with interplanar distances larger than the *d*-spacing of the (111) plane of fcc β-PdH_x in 1−2 nm-sized particles implied possible nucleation pathways for nonfcc seeds (Figure S24).

To evaluate the influence of H_2 gas over electrochemically formed H species in the development of a nonfcc phase, relatively positive electric potentials of 0, −0.55, and −0.8 V vs Ag/AgCl were applied to Pd solution with H_2 gas bubbled simultaneously. The supply of external H_2 facilitated the formation of the metastable phase and increased the observation probability of the nonfcc phase by ∼10% in all three conditions (Figures S20c and S25). However, it was not as productive as the electrochemical approach with more negative electric potentials, which can be seen to be superior for the synthesis of the metastable phase (Figure 6a,b). Considering that the degree of supersaturation of H_2 near the electrode surface reaches 9.3 during HER in a 0.1 M H_2SO_4 solution at 25 °C, which corresponds to 7.2 mM, while the saturation concentration in water is ∼0.75 mM,[21,22] different amounts of hydrogen near an electrode in the two systems could be the cause of the distinction.

2.5. Effect of Electrochemical Variables on the Electrosynthesis of Nonfcc Particles. For the investigation of electrochemical conditions that promote the formation of the nonfcc phase on electrodes, the four variables of current density, electrodeposition time, Pd concentration, and solution pH, were controlled. Although the comparison of electrochemical reduction and the H_2 bubbling system inferred the correlation between the nonfcc phase and H-to-Pd ratio in solution, the fractions of the nonfcc phase in single isolated and one side-coalesced single-crystalline particles were reasonably consistent at around 50% regardless of the experimental conditions at pH 3.3 (Figure 6a,b). While the total volume fraction of the nonfcc phase on electrodes was estimated to be at most ∼20% as nonfcc was rarely observed in agglomerates and polycrystalline particles (Figure 6c,d), increasing current density or deposition time failed to bring about notable differences, though longer deposition time resulted in slightly more number of larger agglomerates (Figures S26 and S27). Higher current density conditions assumedly contributed to the enhanced H_2 bubble nucleation rate rather than increasing the supersaturation level of H_2 or the amount of hydrogen that can incorporate into Pd. Likewise, a longer deposition time would have affected the total volume of generated H_2, not the supersaturation level.

However, the total volume fraction was highly dependent on Pd concentration and pH of the solution; the total fraction was inversely proportional to Pd concentration (Figure 6d), and the nonfcc phase was exclusively observed in acidic solutions (Figure S28). Higher Pd concentration increased the flux of the Pd ion diffusing toward an electrode, and it led to a greater number of bigger agglomerates (Figure S29). Dependency on pH can be ascribed to polynuclear hydroxo complexes (PHC, $[Pd(OH)_2]_n$) formed by the hydrolysis of Pd ions in neutral and basic solutions.[23−25] The larger size of PHC could have facilitated the formation of aggregated Pd nanoparticles[23] where the nonfcc structure rarely survives.

3. CONCLUSIONS

In this study, we discovered unique metastable nonfcc PdH_x nanoparticles through a synthesis route relying on electrochemical coreduction of Pd ions and water. AET-based unit cell approximation revealed a possible triclinic loose-packed structure of the nonfcc phase. The low observance probability of the nonfcc phase in single-crystalline particles that were merged with others on multiple sides, as well as polycrystalline particles, showed the vulnerability of the metastable phase upon atom rearrangement triggered by coalescence. For further characterization and utilization of this metastable phase, the development of a method that facilitates the dominant production of isolated single-crystalline particles should be pursued. The findings of this work can provide fundamental insight into the in situ production of metastable phases, which, on the long-term, can potentially be of interest for catalytic or materials applications.

■ ASSOCIATED CONTENT

Supporting Information

The Supporting Information is available free of charge at https://pubs.acs.org/doi/10.1021/jacs.4c04826.

Experimental details, chronopotentiometry curve, additional EELS spectra, SAED pattern, tilt series, reconstructed atomic structure, unit cell candidate structure and simulated diffraction patterns, particle heat treatment, electrodeposition potential control, H_2 gas bubbling effect, carbon nanotube electrode effect, comparison of Pt and graphite counter electrode, small particle analysis, TEM grid electrode configuration, distribution of particles depending on current density, deposition time, pH, and Pd concentration (PDF)

■ AUTHOR INFORMATION

Corresponding Author

Xiao Su − *Department of Chemical and Biomolecular Engineering, University of Illinois at Urbana−Champaign, Urbana, Illinois 61801, United States;* orcid.org/0000-0001-7794-290X; Email: x2su@illinois.edu

https://doi.org/10.1021/jacs.4c04826
J. Am. Chem. Soc. 2024, 146, 18586−18591

Author

Jaeyoung Hong − *Department of Chemical and Biomolecular Engineering, University of Illinois at Urbana−Champaign, Urbana, Illinois 61801, United States; Department of Materials and Science Engineering, University of Illinois at Urbana−Champaign, Champaign, Illinois 61801, United States;* orcid.org/0000-0001-9605-8888

Complete contact information is available at: https://pubs.acs.org/10.1021/jacs.4c04826

Author Contributions

The manuscript was written through contributions of all authors. All authors have given approval to the final version of the manuscript.

Notes

The authors declare no competing financial interest.

■ ACKNOWLEDGMENTS

This work was primarily supported by the NSF DMR/DMREF grant #2323988. TEM analysis was carried out in the Materials Research Laboratory Central Research Facilities, University of Illinois. The authors thank John Miao and Minh Pham from the University of California at Los Angeles for helping with running RESIRE algorithm-based AET.

■ ABBREVIATIONS

fcc, face-centered cubic; hcp, hexagonal close-packed; nonfcc, not face-centered cubic; HER, hydrogen evolution reaction; TEM, transmission electron microscopy; STEM, scanning transmission electron microscopy; EDS, energy-dispersive X-ray spectroscopy; EELS, electron energy loss spectroscopy; fft, fast Fourier transform; AET, atomic electron tomography; CNT, carbon nanotube; PHC, polynuclear hydroxo complexes

■ REFERENCES

(1) Hong, J.; Bae, J.-H.; Jo, H.; Park, H.-Y.; Lee, S.; Hong, S. J.; Chun, H.; Cho, M. K.; Kim, J.; Kim, J.; et al. Metastable hexagonal close-packed palladium hydride in liquid cell TEM. *Nature* **2022**, *603* (7902), 631−636.

(2) Haynes, W. M. *CRC Handbook of Chemistry and Physics*; CRC Press, 2016.

(3) Hussein, H. E.; Amari, H.; Breeze, B. G.; Beanland, R.; Macpherson, J. V. Controlling palladium morphology in electrodeposition from nanoparticles to dendrites via the use of mixed solvents. *Nanoscale* **2020**, *12* (42), 21757−21769.

(4) Reyes-Gasga, J.; Gómez-Rodríguez, A.; Gao, X.; José-Yacamán, M. On the interpretation of the forbidden spots observed in the electron diffraction patterns of flat Au triangular nanoparticles. *Ultramicroscopy* **2008**, *108* (9), 929−936.

(5) Baldi, A.; Narayan, T. C.; Koh, A. L.; Dionne, J. A. In situ detection of hydrogen-induced phase transitions in individual palladium nanocrystals. *Nat. Mater.* **2014**, *13* (12), 1143−1148.

(6) Niu, Y.; Liu, X.; Wang, Y.; Zhou, S.; Lv, Z.; Zhang, L.; Shi, W.; Li, Y.; Zhang, W.; Su, D. S.; et al. Visualizing Formation of Intermetallic PdZn in a Palladium/Zinc Oxide Catalyst: Interfacial Fertilization by PdH_x. *Angew. Chem., Int. Ed.* **2019**, *58* (13), 4232−4237.

(7) Yang, Y.; Zhou, J.; Zhu, F.; Yuan, Y.; Chang, D. J.; Kim, D. S.; Pham, M.; Rana, A.; Tian, X.; Yao, Y.; et al. Determining the three-dimensional atomic structure of an amorphous solid. *Nature* **2021**, *592* (7852), 60−64.

(8) Yuan, Y.; Kim, D. S.; Zhou, J.; Chang, D. J.; Zhu, F.; Nagaoka, Y.; Yang, Y.; Pham, M.; Osher, S. J.; Chen, O.; et al. Three-dimensional atomic packing in amorphous solids with liquid-like structure. *Nat. Mater.* **2022**, *21* (1), 95−102.

(9) Arblaster, J. W. Crystallographic properties of palladium. *Platinum Met. Rev.* **2012**, *56* (3), 181−189.

(10) Liao, H.-G.; Cui, L.; Whitelam, S.; Zheng, H. Real-time imaging of Pt3Fe nanorod growth in solution. *Science* **2012**, *336* (6084), 1011−1014.

(11) Jose-Yacaman, M.; Gutierrez-Wing, C.; Miki, M.; Yang, D.-Q.; Piyakis, K.; Sacher, E. Surface diffusion and coalescence of mobile metal nanoparticles. *J. Phys. Chem. B* **2005**, *109* (19), 9703−9711.

(12) Grammatikopoulos, P.; Cassidy, C.; Singh, V.; Sowwan, M. Coalescence-induced crystallisation wave in Pd nanoparticles. *Sci. Rep.* **2014**, *4* (1), 5779.

(13) de Chialvo, M. G.; Chialvo, A. Hydrogen evolution reaction: Analysis of the Volmer-Heyrovsky-Tafel mechanism with a generalized adsorption model. *J. Electroanal. Chem.* **1994**, *372* (1−2), 209−223.

(14) Filhol, J. S.; Neurock, M. Elucidation of the electrochemical activation of water over Pd by first principles. *Angew. Chem.* **2006**, *118* (3), 416−420.

(15) Krischer, K.; Savinova, E. R. Fundamentals of electrocatalysis. *Handbook of Heterogeneous Catalysis: Online*; Wiley, 2008, 1873−1905..

(16) Zhang, L.; Chang, Q.; Chen, H.; Shao, M. Recent advances in palladium-based electrocatalysts for fuel cell reactions and hydrogen evolution reaction. *Nano Energy* **2016**, *29*, 198−219.

(17) Rampino, L. D.; Nord, F. Preparation of palladium and platinum synthetic high polymer catalysts and the relationship between particle size and rate of hydrogenation. *J. Am. Chem. Soc.* **1941**, *63* (10), 2745−2749.

(18) Nakatsuji, H.; Hada, M. Interaction of a hydrogen molecule with palladium. *J. Am. Chem. Soc.* **1985**, *107* (26), 8264−8266.

(19) Loh, N. D.; Sen, S.; Bosman, M.; Tan, S. F.; Zhong, J.; Nijhuis, C. A.; Král, P.; Matsudaira, P.; Mirsaidov, U. Multistep nucleation of nanocrystals in aqueous solution. *Nat. Chem.* **2017**, *9* (1), 77−82.

(20) Dachraoui, W.; Henninen, T. R.; Keller, D.; Erni, R. Multi-step atomic mechanism of platinum nanocrystals nucleation and growth revealed by in-situ liquid cell STEM. *Sci. Rep.* **2021**, *11* (1), 23965.

(21) Dapkus, K. V.; Sides, P. J. Nucleation of electrolytically evolved hydrogen at an ideally smooth electrode. *J. Colloid Interface Sci.* **1986**, *111* (1), 133−151.

(22) Angulo, A.; van der Linde, P.; Gardeniers, H.; Modestino, M.; Fernández Rivas, D. Influence of bubbles on the energy conversion efficiency of electrochemical reactors. *Joule* **2020**, *4* (3), 555−579.

(23) Kettemann, F.; Wuithschick, M.; Caputo, G.; Kraehnert, R.; Pinna, N.; Rademann, K.; Polte, J. Reliable palladium nanoparticle syntheses in aqueous solution: the importance of understanding precursor chemistry and growth mechanism. *CrystEngComm* **2015**, *17* (8), 1865−1870.

(24) Soreta, T. R.; Strutwolf, J.; O'Sullivan, C. K. Electrochemically deposited palladium as a substrate for self-assembled monolayers. *Langmuir* **2007**, *23* (21), 10823−10830.

(25) Simonov, P.; Troitskii, S. Y.; Likholobov, V. Preparation of the Pd/C catalysts: A molecular-level study of active site formation. *Kinet. Catal.* **2000**, *41*, 255−269.